

Electronic Supplementary Information

Variation of counter quaternary ammonium cations and cross-linkers of anionic cage germanoxanes as building blocks of nanoporous materials

Taiki Hayashi,^a Naoto Sato,^a Hiroaki Wada,^{a,b} Atsushi Shimojima,^{*a,b} and Kazuyuki Kuroda ^{*a,b}

^a Department of Applied Chemistry, Faculty of Science and Engineering, Waseda University,
3-4-1 Okubo, Shinjuku-ku, Tokyo 169-8555, Japan

^b Kagami Memorial Research Institute for Materials Science and Technology, Waseda University,
2-8-26 Nishiwaseda, Shinjuku-ku, Tokyo 169-0051, Japan

Table of contents

1. Experimental details

1.1 Materials.....	S3
1.2 Preparation of GSN-2a	S3
1.3 Cation exchange of GSN-1a and GSN-2a with TMA.....	S3
1.4 Cation exchange of GSN-1a with TBA.....	S3
1.5 Preparation of GSN-1b	S3
1.6 Preparation of GSN-1c	S4
1.7 Preparation of GSN-1d	S4
1.8 Cation exchange of GSN-1c and GSN-1d with TMA.....	S4
1.9 Characterization.....	S4

2. Data

Fig. S1 ^{19}F NMR and ^{29}Si NMR spectra, and ESI mass spectrum of TBA-GeD4R	S6
Fig. S2 Powder XRD patterns of TEA-GeD4R and TBA-GeD4R	S7
Fig. S3 Optimized crystal structural model of TBA-GeD4R viewed from <i>a</i> , <i>b</i> , and <i>c</i> axes.....	S8
<i>The interpretation of the crystal structure of TBA-GeD4R</i>	S9
Fig. S4 Simplified structural models of TEA-GeD4R and TBA-GeD4R viewed from <i>a</i> axis.....	S9
Fig. S5 FT-IR spectra of TBA-GeD4R , Q_8M_8 , and GSN-2a	S10
Fig. S6 ^{13}C CP/MAS NMR and ^{29}Si MAS NMR spectra of GSN-2a	S10
Fig. S7 SEM images of GSN-1a and GSN-2a	S11
Fig. S8 FT-IR spectra of TMA-GSN-1a and TMA-GSN-2a	S11
Fig. S9 ^{29}Si MAS NMR spectra of TMA-GSN-1a and TMA-GSN-2a	S12
Fig. S10 ^{13}C MAS NMR spectra of TMA-GSN-1a and TMA-GSN-2a	S12
<i>Calculation of the molar ratio of NCH_3 of TMA and SiCH_3 of cage compounds</i>	S13
Fig. S11 SEM images of TMA-GSN-1a and TMA-GSN-2a	S13
Fig. S12 Simplified structural models of cyclic structures generated from two cage compounds and four cage compounds.....	S14
Fig. S13 FT-IR, ^{29}Si MAS NMR, and ^{13}C MAS NMR spectra, and N_2 adsorption–desorption isotherms of TBA-GSN-1a	S15
Fig. S14 FT-IR spectra of TEA-GeD4R , Q_8M_8 , GSN-1a , T_8 , GSN-1b , D_4 , GSN-1c , M_2 , and GSN-1d	S16
Fig. S15 ^{29}Si MAS NMR spectra of GSN-1a , GSN-1b , GSN-1c , and GSN-1d	S17
<i>The interpretation of the FT-IR and ^{29}Si MAS NMR spectra of GSN-1b, GSN-1c, and GSN-1d</i>	S18
Fig. S16 Pore size distribution of GSN-1b	S19
Fig. S17 FT-IR spectra of TMA-GSN-1c and TMA-GSN-1d	S19
Fig. S18 ^{13}C MAS NMR spectra of TMA-GSN-1c and TMA-GSN-1d	S20
Fig. S19 N_2 adsorption–desorption isotherms of TMA-GSN-1c	S20
Fig. S20 XRD patterns of GSN-1c and GSN-1c with a drop of ethanol.....	S21
Fig. S21 FT-IR spectra of GSN-1a and GSN-2a treated with a mixed solution of TMACl , ethanol, and H_2O	S21
Fig. S22 TG-DTA curves of GSN-1a , GSN-2a , TMA-GSN-1a , and TMA-GSN-2a	S22
References	S22

1. Experimental details

1.1 Materials

The following reagents were used without purification: Ethanol (super dehydrated, FUJIFILM Wako Pure Chemical Corp., >99.5%), hexane (Kanto Chemical Co. Inc., >95.0%), platinum(0)-1,3-divinyl-1,1,3,3-tetramethyldisiloxane complex solution in xylene (Karstedt's catalyst solution, Pt ~2%, Sigma-Aldrich), tetrabutylammonium bromide (TBABr, Tokyo Chemical Industry Co. Ltd., >98.0%), tetrabutylammonium chloride (TBACl, Sigma-Aldrich, ≥97.0%), tetramethylammonium chloride (TMACl, Tokyo Chemical Industry Co. Ltd., >98.0%), 1,1,3,3-tetramethyldisiloxane (M₂, Tokyo Chemical Industry Co. Ltd., >97.0%), 2,4,6,8-tetramethylcyclotetrasiloxane (D₄, Tokyo Chemical Industry Co. Ltd., >95.0%), and toluene (super dehydrated, FUJIFILM Wako Pure Chemical Corp., >99.5%). **TEA-GeD₄R**,¹ Q₈M₈,² and **GSN-1a**¹ were synthesized by the methods reported previously by us. Octa(hydridosilsesquioxane) (T₈) was synthesized according to literature procedures.³

1.2 Preparation of GSN-2a

TBA-GeD₄R (0.10 g, 0.054 mmol) and Q₈M₈ (0.056 g, 0.055 mmol) were dissolved in toluene (40 mL), followed by the addition of Karstedt's catalyst solution (38.6 μL). After stirring the mixture for 1 d at 80 °C, the gel-like precipitate was recovered by filtration, washed with toluene and hexane, and dried under reduced pressure to give **GSN-2a** as a grey powder (0.14 g, 90%).

1.3 Cation exchange of GSN-1a and GSN-2a with TMA

TMACl (6.2 g) was added to ethanol (40 mL) to obtain a saturated solution containing a small amount of undissolved TMACl. **GSN-1a** (0.11 g) or **GSN-2a** (0.12 g) was added to this solution. After stirring the mixture for 2 d at room temperature, the precipitate was recovered via filtration, washed with ethanol and hexane, and dried under reduced pressure. The products were denoted as **TMA-GSN-1a** and **TMA-GSN-2a**, respectively.

1.4 Cation exchange of GSN-1a with TBA

TBACl (6.4 g) was added to ethanol (40 mL) to obtain an ethanol solution of TBACl. **GSN-1a** (0.11 g) was added to the resulting solution. After stirring the mixture for 2 d at room temperature, the precipitate was recovered via filtration, washed with ethanol and hexane, and dried under reduced pressure. The product was denoted as **TBA-GSN-1a**.

1.5 Preparation of GSN-1b

TEA-GeD₄R (0.15 g, 0.087 mmol) and T₈ (0.036 g, 0.085 mmol) were dissolved in toluene (40 mL), followed by the addition of Karstedt's catalyst solution (38.6 μL). After stirring the mixture for 1 d at 80 °C, the precipitated product was recovered by filtration, washed with toluene and hexane, and dried under reduced pressure to give **GSN-1b** as a white solid (0.13 g, 70%).

1.6 Preparation of GSN-1c

TEA-GeD4R (0.15 g, 0.087 mmol) and **D₄** (42.1 μ L, 0.18 mmol) were dissolved in toluene (40 mL), followed by the addition of Karstedt's catalyst solution (38.6 μ L). After stirring the mixture for 1 d at 80 °C, the precipitated product was recovered by filtration, washed with toluene and hexane, and dried under reduced pressure to give **GSN-1c** as a pale–yellow solid (0.091 g, 47%).

1.7 Preparation of GSN-1d

TEA-GeD4R (0.15 g, 0.087 mmol) and **M₂** (61.2 μ L, 0.35 mmol) were dissolved in toluene (40 mL), followed by the addition of Karstedt's catalyst solution (38.6 μ L). After stirring the mixture for 1 d at 80 °C, the solvent was removed at 80 °C under reduced pressure to give a yellow–brown solid. The solid was washed with hexane, recovered via centrifugation, and dried under reduced pressure to give **GSN-1d** as a yellow–brown solid (0.091 g, 46%).

1.8 Cation exchange of GSN-1c and GSN-1d with TMA

GSN-1c (0.11 g) or **GSN-1d** (0.10 g) was added to a saturated solution of TMACl in ethanol (40 mL). After stirring the mixture for 2 d at room temperature, the precipitate was recovered via filtration, washed with ethanol and hexane, and dried under reduced pressure. The products were denoted as **TMA-GSN-1c** and **TMA-GSN-1d**, respectively.

1.9 Characterization

Liquid-state ¹H, ¹³C, ¹⁹F, and ²⁹Si nuclear magnetic resonance (NMR) spectra were recorded on a JEOL JNM ECZ 500 spectrometer at resonance frequencies of 500.16, 125.77, 470.62, and 99.37 MHz, respectively at ambient temperature using 5 mm glass tubes. Tetramethylsilane was used as an internal reference ($\delta = 0$ ppm) for ¹H, ¹³C, and ²⁹Si NMR spectroscopy. Trifluoromethylbenzene was used as an internal reference ($\delta = -62.88$ ppm)⁴ for ¹⁹F NMR spectroscopy. Toluene-*d*₈ was used to obtain lock signals. A small amount of Cr(acac)₃ (acac = acetylacetonate) was used as a relaxation agent for ²⁹Si nuclei. The ²⁹Si NMR spectra were measured with a 45° pulse and recycle delay of 10 s. Solid-state NMR spectra were recorded on a JEOL JNM ECA 400 spectrometer or a JEOL JNM ECX 400 spectrometer under the optimal conditions for each sample and equipment (Details are shown below.). The solid-state ¹³C cross-polarization magic angle spinning (CP/MAS) NMR spectrum of **GSN-2a** was recorded on a JEOL JNM ECA 400 spectrometer at a resonance frequency of 100.53 MHz with a contact time of 5 ms and recycle delay of 10 s at ambient temperature. The sample was placed in a 5 mm zirconia rotor and spun at 8 kHz. The solid-state ¹³C CP/MAS NMR spectra of **GSN-1a**, **TMA-GSN-1a**, and **TMA-GSN-2a** were recorded on a JEOL JNM ECX 400 spectrometer at a resonance frequency of 99.54 MHz with a contact time of 5 ms and recycle delay of 10 s at ambient temperature. The samples were placed in a 4 mm silicon nitride rotor and spun at 6 kHz. The solid-state ¹³C MAS NMR spectra of **TMA-GSN-1a** and **TMA-GSN-2a** were recorded on a JEOL JNM ECA 400 spectrometer at a resonance frequency of 100.53 MHz and recycle delay of 15 s at ambient temperature. The samples were placed in a 5 mm zirconia rotor and spun at 8 kHz. The solid-state ¹³C MAS NMR spectra of **TMA-GSN-1c** and **TMA-GSN-1d** were recorded on a JEOL JNM ECX 400 spectrometer

at a resonance frequency of 99.54 MHz and recycle delay of 15 s at ambient temperature. The samples were placed in a 4 mm silicon nitride rotor and spun at 6 kHz. The solid-state ^{29}Si MAS NMR spectra of **GSN-2a**, **TMA-GSN-1a**, **TMA-GSN-2a**, **GSN-1b**, **GSN-1c**, and **GSN-1d** were recorded on a JEOL JNM ECA 400 spectrometer at a resonance frequency of 79.43 MHz with 90° pulse and recycle delay of 500 s at ambient temperature. The samples were placed in a 5 mm zirconia rotor and spun at 8 kHz. The solid-state ^{29}Si MAS NMR spectrum of **TMA-GSN-2a** was recorded on a JEOL JNM ECX 400 spectrometer at a resonance frequency of 78.65 MHz with a 90° pulse and recycle delay of 500 s at ambient temperature. The sample was placed in a 4 mm zirconia rotor and spun at 6 kHz. Hexamethylbenzene was used as an external reference ($\delta = 17.4$ ppm) for solid-state ^{13}C NMR and poly(dimethylsilane) was used as an external reference ($\delta = -33.8$ ppm) for solid-state ^{29}Si NMR spectroscopy. Electrospray ionization mass spectrometry (ESI-MS) was carried out on a JEOL JMS T100 CS AccuTOF spectrometer. Fourier transform infrared (FT-IR) spectroscopy was carried out on a JASCO FT/IR-6100 spectrometer. The FT-IR spectra of solid samples were obtained using the KBr method. Liquid samples (M_2 and D_4) are sandwiched between two KBr plates to obtain their IR spectra. CHN elemental analysis was conducted using a PerkinElmer PE2400 II instrument. Powder X-ray diffraction (XRD) measurements were performed on a Rigaku Rint-Ultima III diffractometer with a parallel beam geometry equipped with a scintillation detector and parabolic multilayer mirror using $\text{Cu K}\alpha$ radiation (40 kV, 40 mA). Single-crystal X-ray structural analysis was performed on a Rigaku RAXIS RAPID diffractometer by using a graphite monochromated $\text{Cu K}\alpha$ ($\lambda = 1.54187 \text{ \AA}$) radiation. DFT calculations for structural refinement of the proposed model obtained by the single-crystal X-ray analysis were conducted by using an BIOVIA Materials Studio system. The CASTEP module was used with the GGA-PBE functional. Structural models were created using VESTA software.⁵ N_2 adsorption–desorption measurements were performed on a Quantachrome Autosorb-iQ at -196°C . The samples were heated at 120°C for 4.5 h under reduced pressure prior to measurement. Pore size distribution was calculated by a quenched solid density functional theory (QSDFT) by using the carbon slit / cylindrical pore model based on previous reports.^{6,7} Scanning electron microscopy (SEM) images were obtained on a Hitachi S5500 electron microscope at an accelerating voltage of 10 or 15 kV. Thermogravimetric and differential thermal analysis (TG-DTA) was conducted on a RIGAKU Thermo plus EV02 instrument under a dry-air flow with a heating rate of 10 K min^{-1} .

2. Data

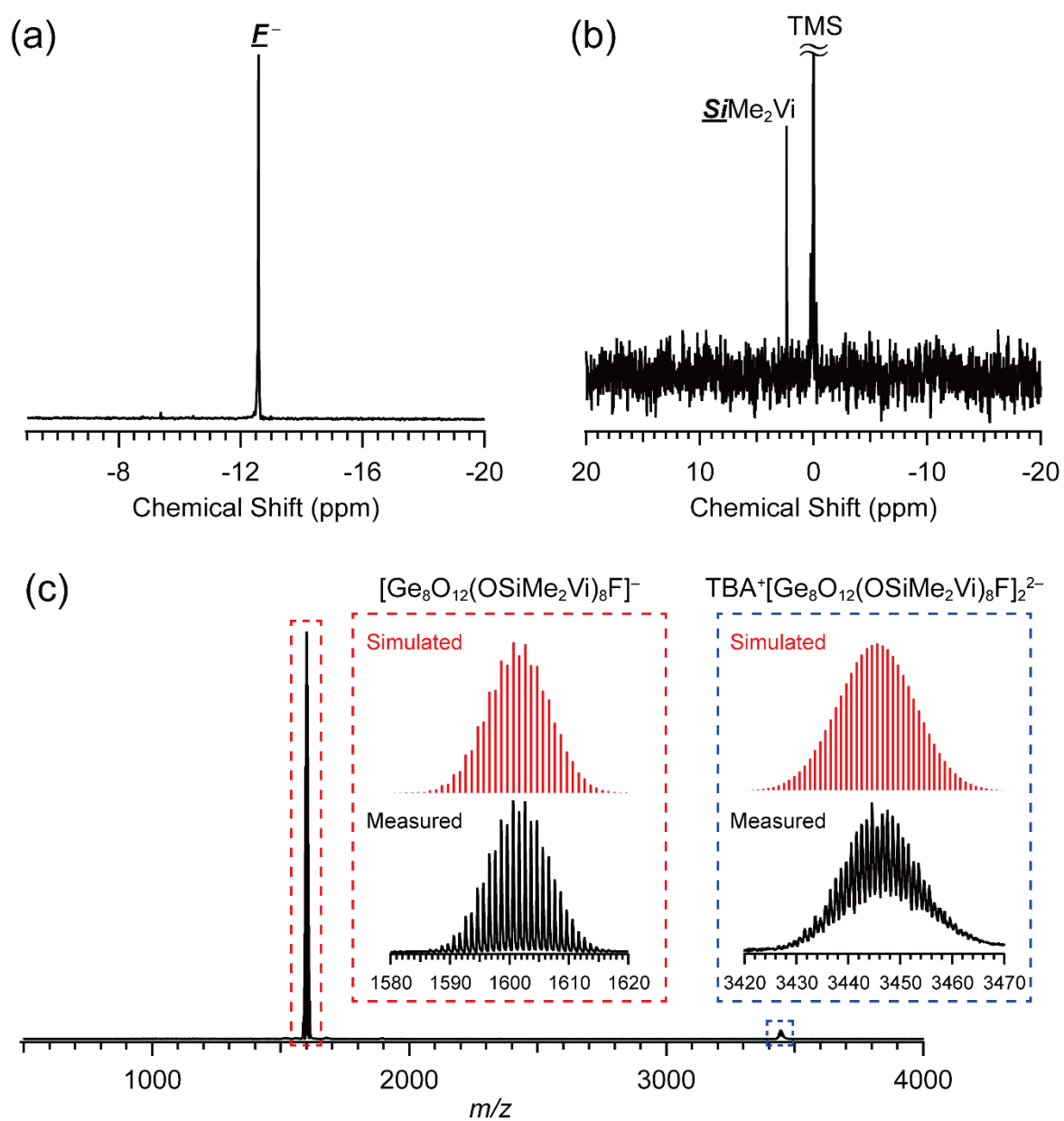


Fig. S1 (a) ^{19}F NMR and (b) ^{29}Si NMR spectra, and (c) ESI mass spectrum of TBA-GeD4R.

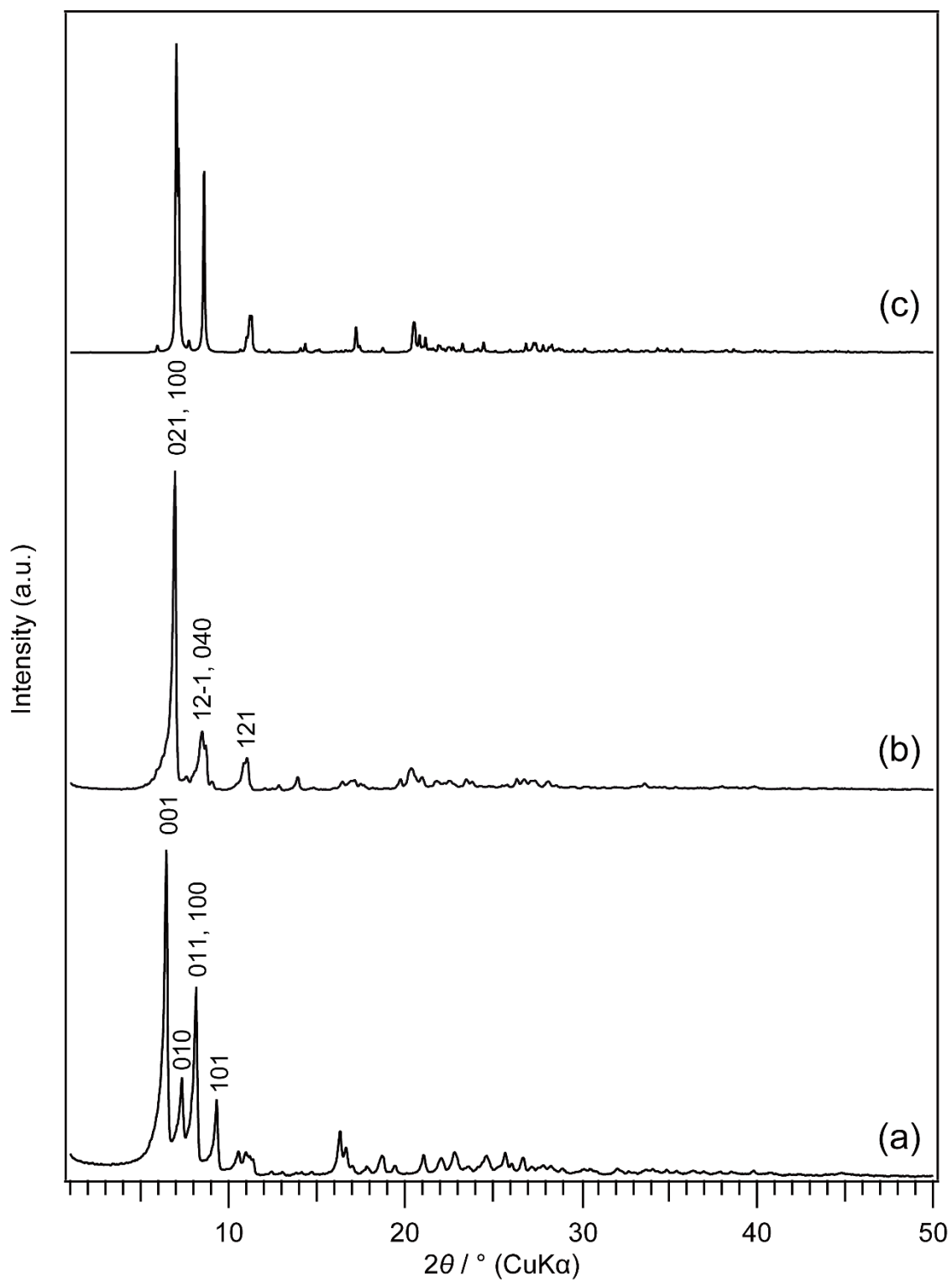


Fig. S2 Powder XRD patterns of (a) **TEA-GeD4R** and (b) **TBA-GeD4R**. (c) Simulation of XRD pattern of the optimized structural model of **TBA-GeD4R**.

Crystal system and unit cell of TBA-GeD4R obtained by single-crystal X-ray structural analysis

Monoclinic, Space Group: $P2_1/m$

$a = 13.10930 \text{ \AA}$, $b = 41.09280 \text{ \AA}$, $c = 16.89670 \text{ \AA}$

$\alpha = 90.0000^\circ$, $\beta = 109.7150^\circ$, $\gamma = 90.0000^\circ$

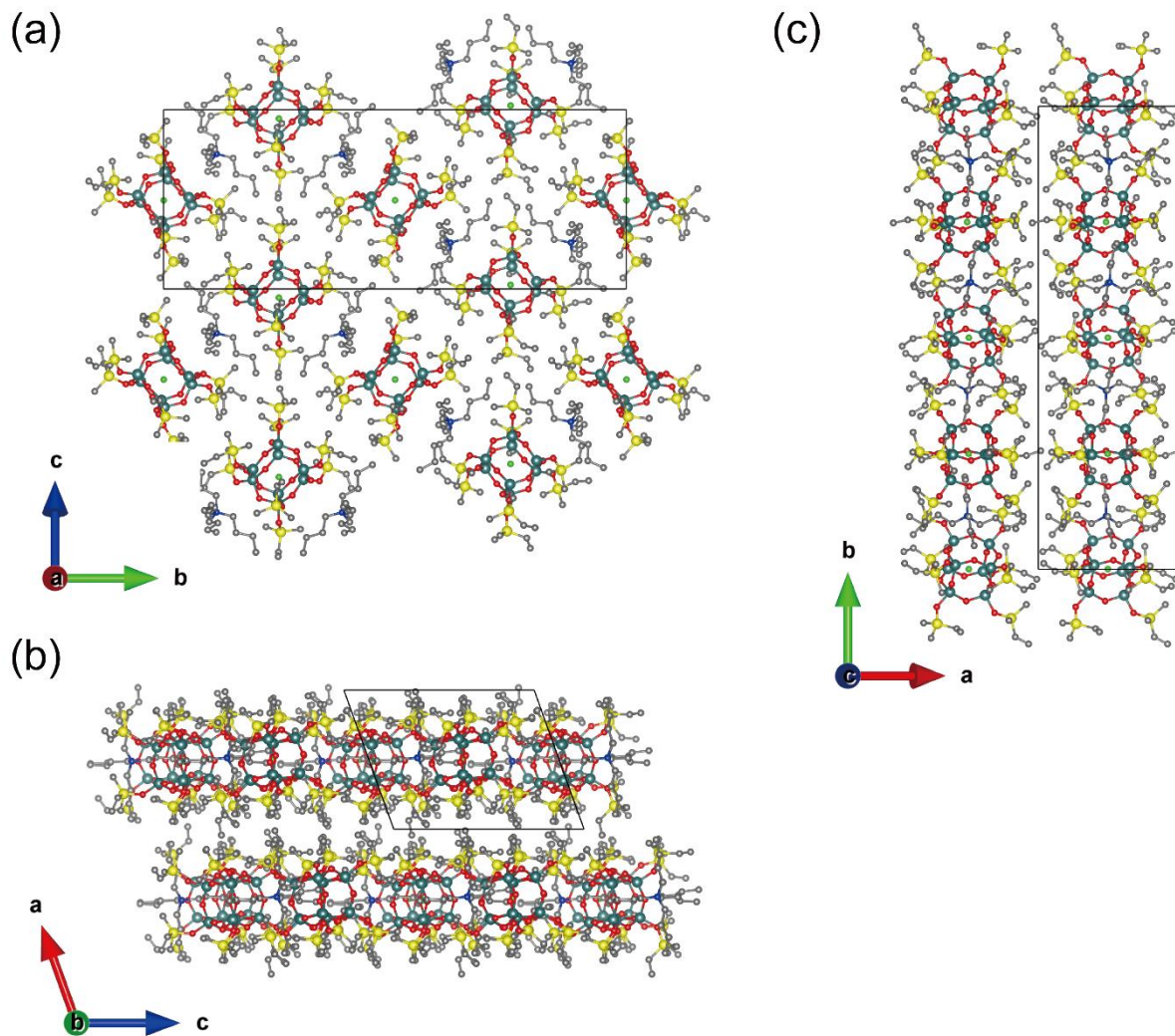


Fig. S3 Optimized crystal structural model of **TBA-GeD4R** viewed from (a) a , (a) b , and (b) c axes. Hydrogen atoms are omitted for clarity. Atom colors: Dark green; Ge, Yellow; Si, Red; O, Blue; N, Light green; F, Gray; C.

The interpretation of the crystal structure of *TBA-GeD4R*.

The crystal structure of **TEA-GeD4R** was determined by our previous report.¹ Crystal structure of **TBA-GeD4R** has not completely been determined by a single-crystal X-ray analysis, but it was enough to calculate the crystal system, unit cell, and location of heavy elements such as germanium and silicon. An initial structural model was prepared from the single crystal X-ray structural analysis result and was optimized using Materials Studio. The optimized structural models of **TBA-GeD4R** are shown in Fig. S3. The Simulation of XRD pattern of the optimized structural model (Fig. S2c) almost coincided with the powder XRD pattern of **TBA-GeD4R** (Fig. S2b).

Both in **TEA-GeD4R** and **TBA-GeD4R**, cage germanoxane anions and counter cations were arranged two-dimensionally in the b - c plane direction, although their different periodicities (Fig. S4). Alkyl chains of the cations were extended in the planes which perpendicular to the b - c planes. The distances between D4R germanoxane cages along the $[100]$ directions, which consistent with the stacking direction of the two-dimensional layered structure of cage germanoxane anions and counter cations, were 1.10 nm (**TEA-GeD4R**) and 1.31 nm (**TBA-GeD4R**), respectively. These results suggested that the expansion of the distance between the layered structures because of bulkier TBA cations compared to TEA cations.

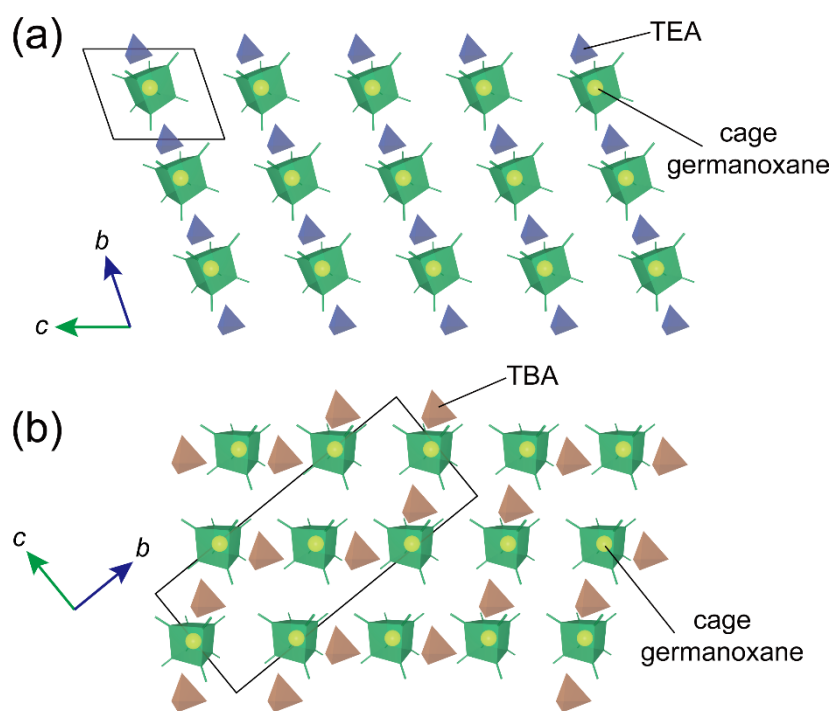


Fig. S4 Simplified structural models of (a) **TEA-GeD4R** and (b) **TBA-GeD4R** viewed from a axis.

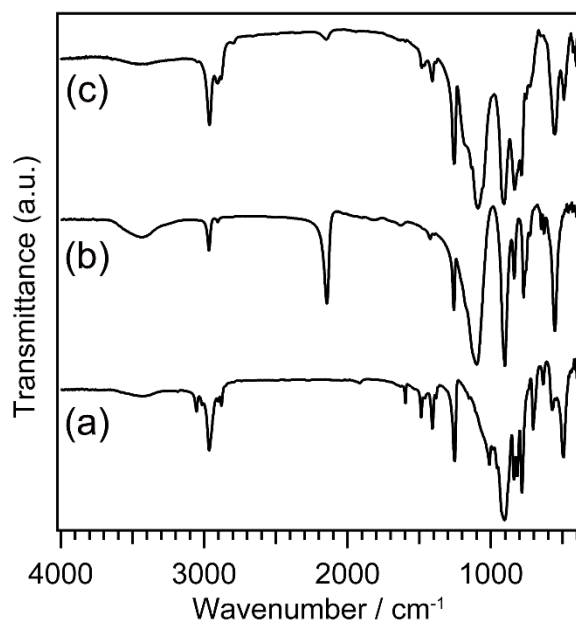


Fig. S5 FT-IR spectra of (a) TBA-GeD4R, (b) Q₈M₈,¹ and (c) GSN-2a.

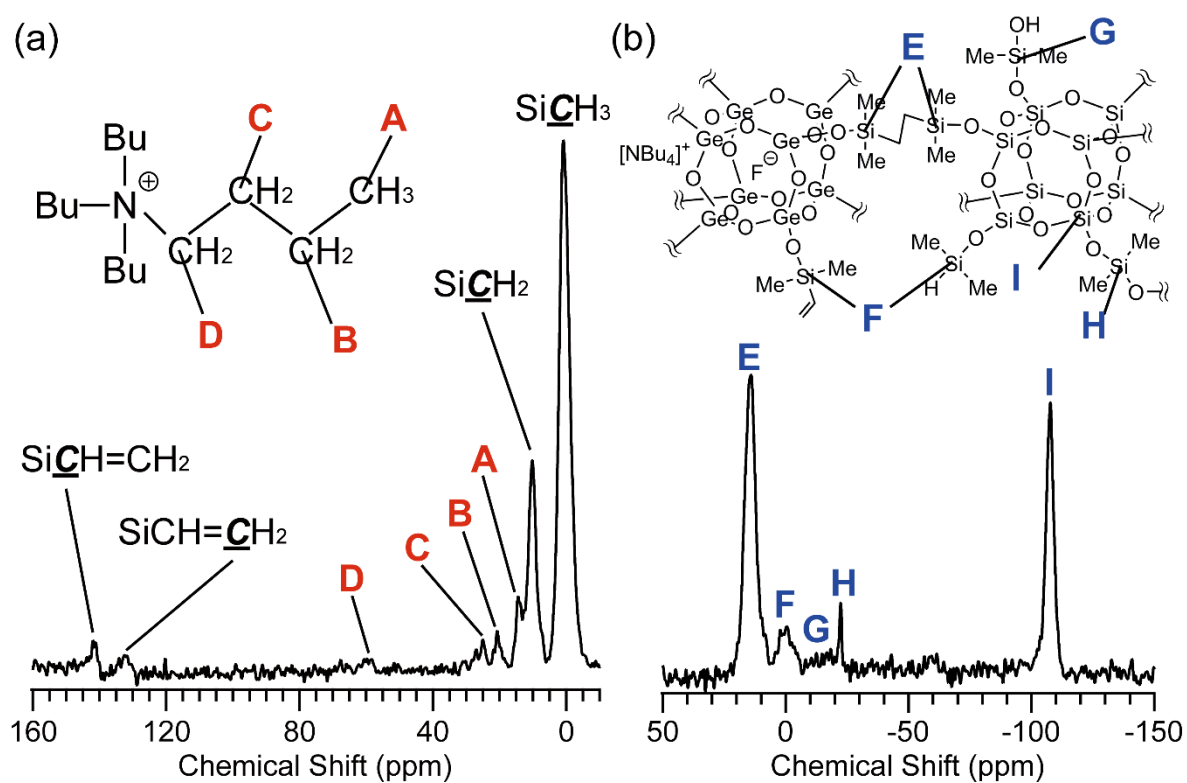


Fig. S6 (a) ¹³C CP/MAS NMR and (b) ²⁹Si MAS NMR spectra of GSN-2a.

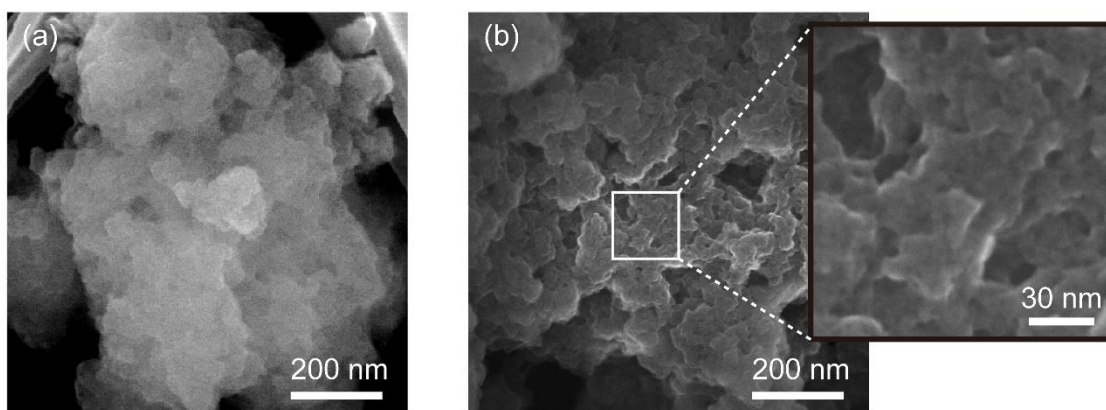


Fig. S7 SEM images of (a) **GSN-1a** and (b) **GSN-2a**.

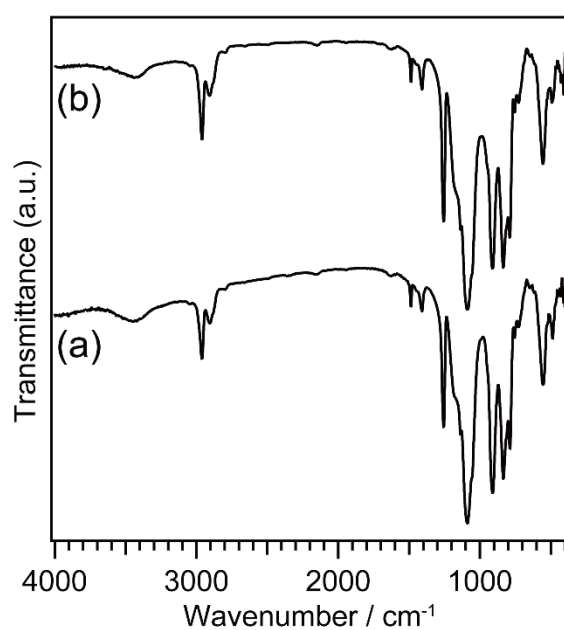


Fig. S8 FT-IR spectra of (a) **TMA-GSN-1a** and (b) **TMA-GSN-2a**.

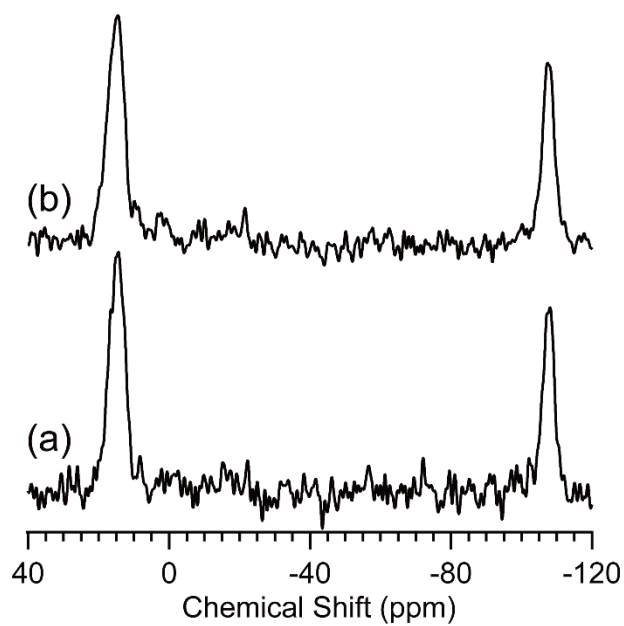


Fig. S9 ^{29}Si MAS NMR spectra of (a) **TMA-GSN-1a** and (b) **TMA-GSN-2a**.

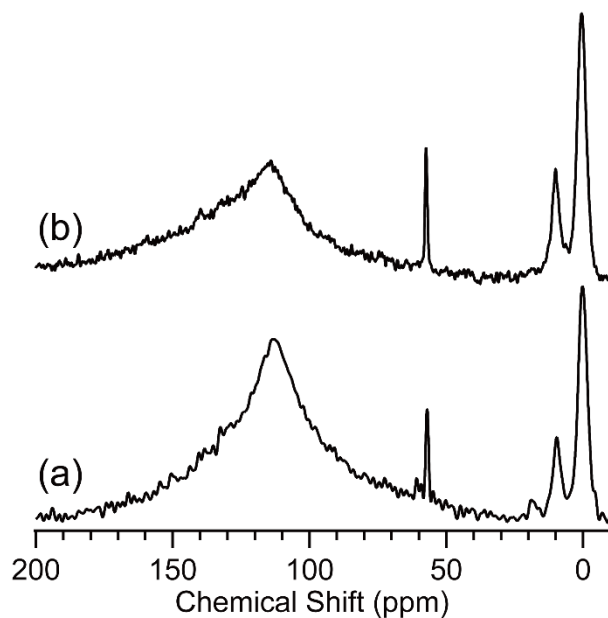


Fig. S10 ^{13}C MAS NMR spectra of (a) **TMA-GSN-1a** and (b) **TMA-GSN-2a**. A broad carbon background signal attributable to the probe was observed at 100–120 ppm due to the low carbon content.

Calculation of the molar ratio of NCH_3 of TMA and $SiCH_3$ of cage compounds.

If preexisting cations (TEA or TBA) in **GSN-1a** and **GSN-2a** were fully exchanged with TMA without any deterioration, the ^{13}C NMR signal integral ratio of NCH_3 of TMA of cage germanoxane to $SiCH_3$ of both cages ($R^{(methyl)}$) was calculated as follows:

$$R^{(methyl)} = \frac{n^{(NCH_3)} \times R^{(cage)}}{n^{(GeOSiCH_3)} \times R^{(cage)} + n^{(SiOSiCH_3)}}$$

where $n^{(NCH_3)}$, $n^{(GeOSiCH_3)}$, $n^{(SiOSiCH_3)}$, $R^{(cage)}$ are the number of methyl groups of TMA cation, silyl groups in cage germanoxane and Q_8M_8 , and the molar ratio of cage germanoxane/ Q_8M_8 , respectively. The values of $n^{(NCH_3)}$, $n^{(GeOSiCH_3)}$, and $n^{(SiOSiCH_3)}$ are 4, 16, 16, respectively. In **GSN-1a**, $R^{(cage)}$ (the molar ratio of **TEA-GeD4R**/ Q_8M_8) is 1.1,¹ and $R^{(methyl)}$ can be calculated to be 1.0/7.6. In **GSN-2a**, $R^{(cage)}$ (the molar ratio of **TBA-GeD4R**/ Q_8M_8) is 1.0, and $R^{(methyl)}$ can be calculated to be 1.0/8.0.

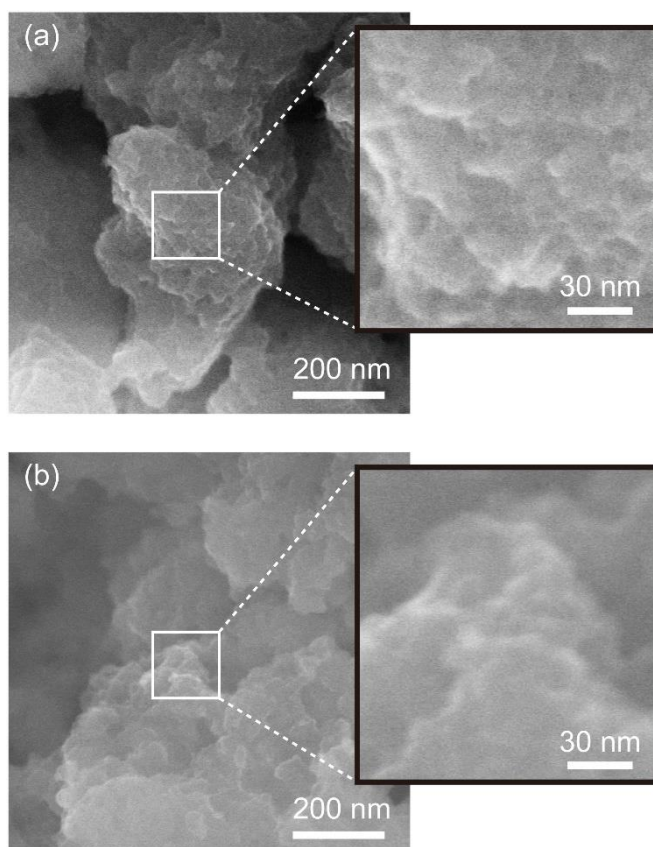


Fig. S11 SEM images of (a) **TMA-GSN-1a** and (b) **TMA-GSN-2a**.

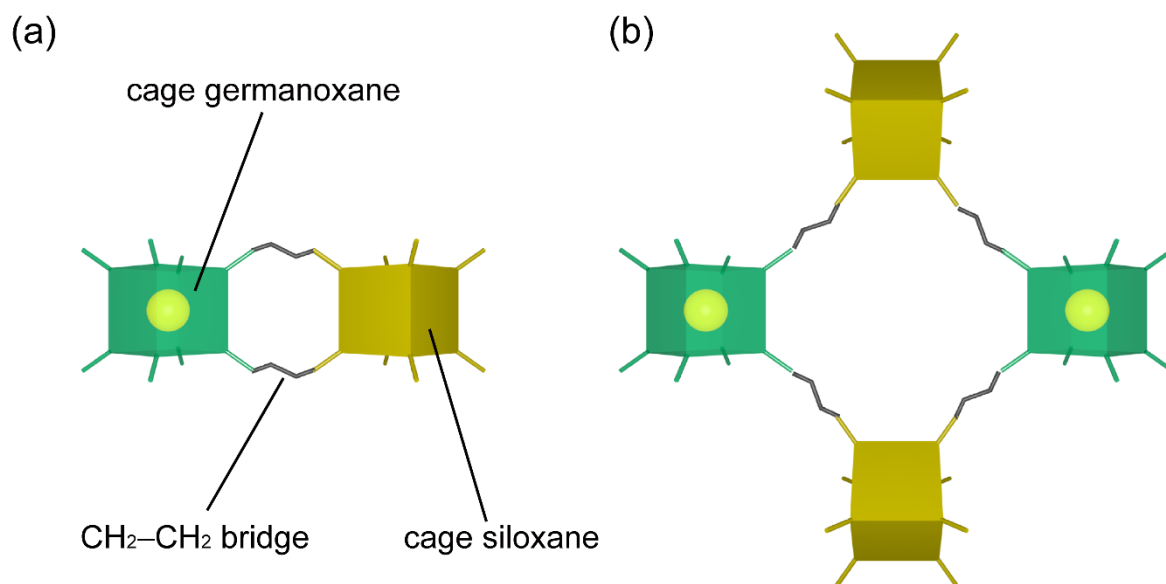


Fig. S12 Simplified structural models of cyclic structures generated from (a) two cage compounds and (b) four cage compounds.

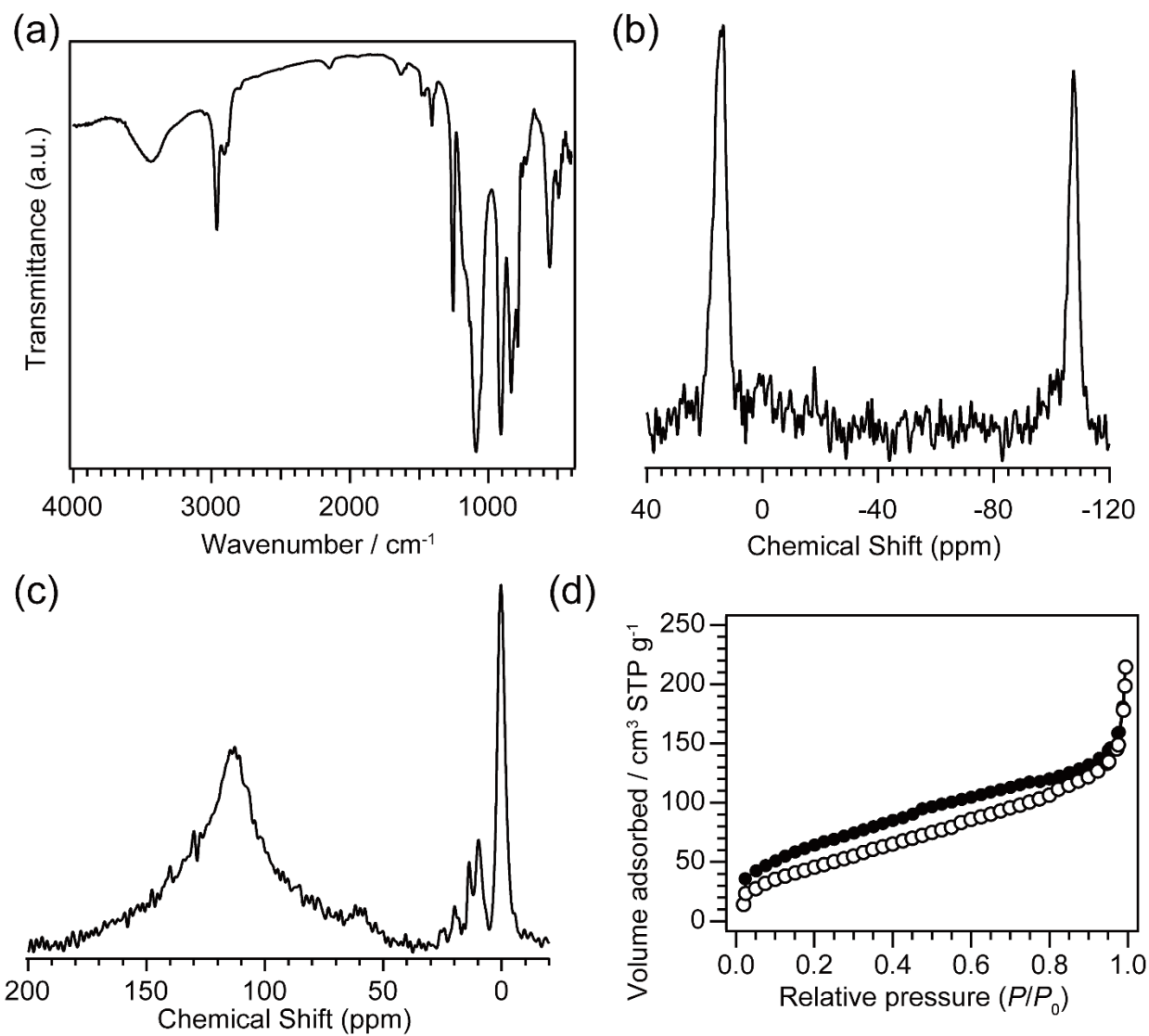


Fig. S13 (a) FT-IR, (b) ²⁹Si MAS NMR, and (c) ¹³C MAS NMR spectra (A broad carbon background signal attributable to probe was observed at 100–120 ppm.), and (d) N₂ adsorption–desorption isotherms (The open and filled symbols denote adsorption and desorption, respectively.) of **TBA-GSN-1a**.

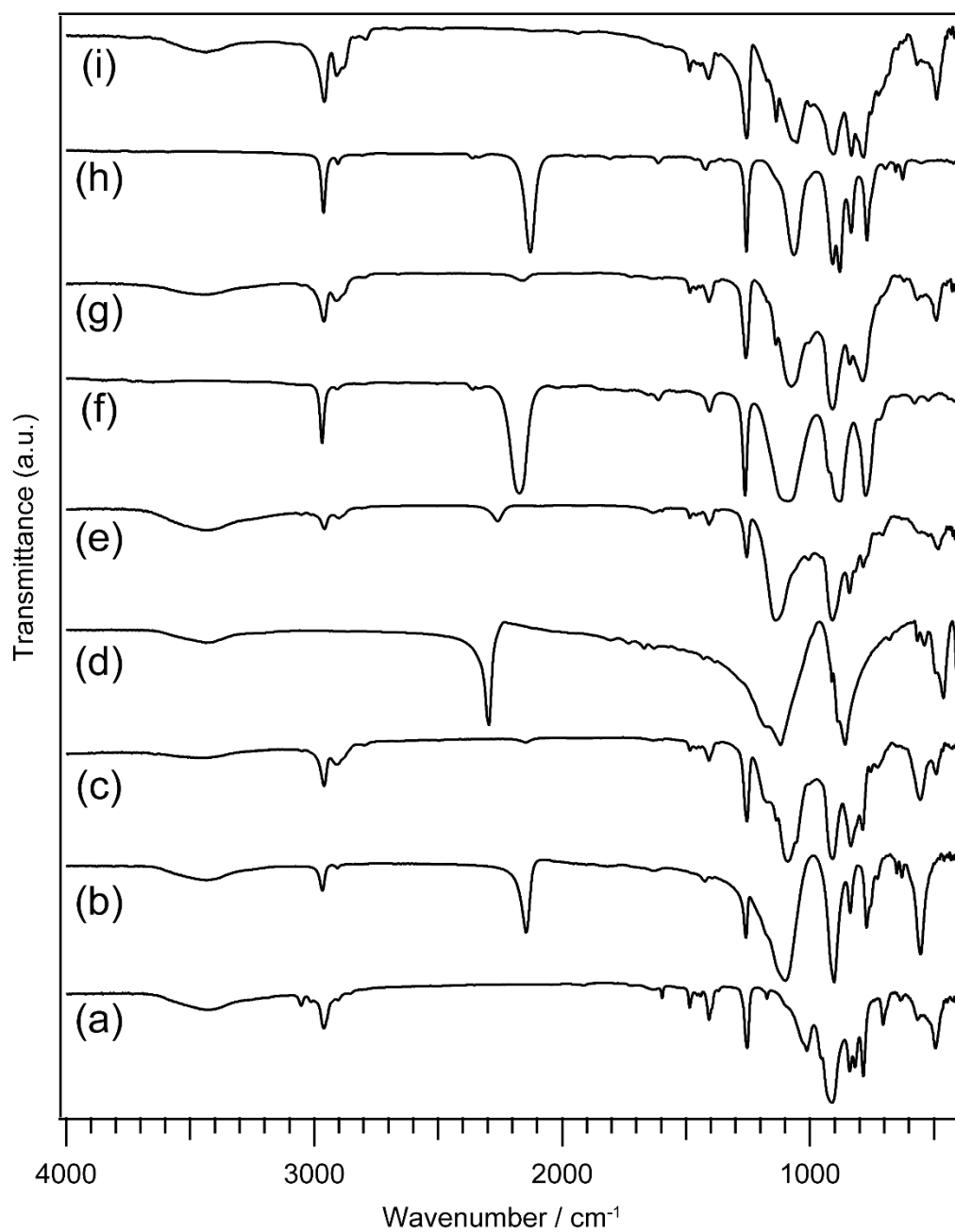


Fig. S14 FT-IR spectra of (a) TEA-GeD4R,¹ (b) Q₈M₈,¹ (c) GSN-1a,¹ (d) T₈, (e) GSN-1b, (f) D₄, (g) GSN-1c, (h) M₂, and (i) GSN-1d.

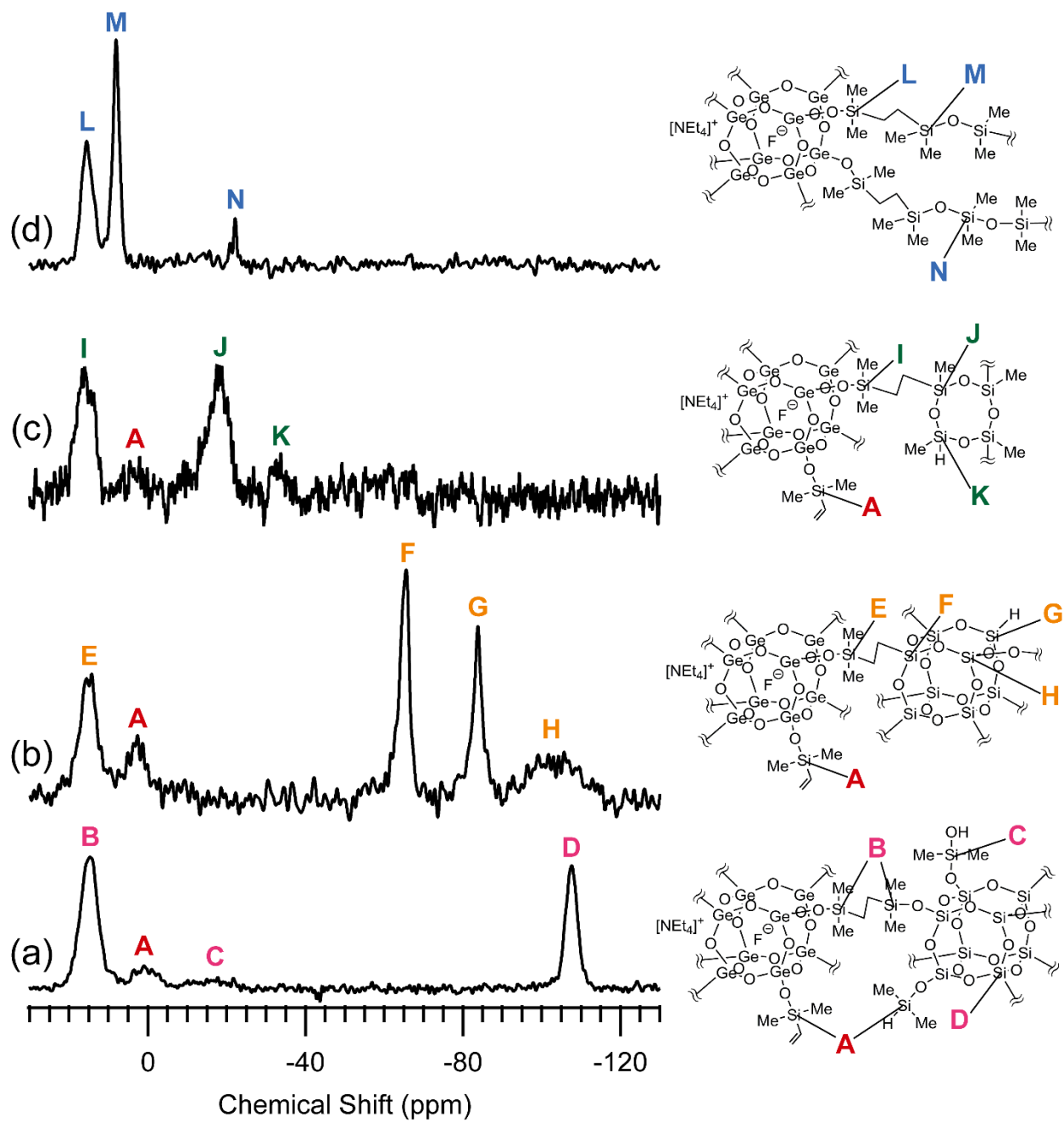


Fig. S15 ^{29}Si MAS NMR spectra of (a) GSN-1a,¹ (b) GSN-1b, (c) GSN-1c, and (d) GSN-1d.

The interpretation of the FT-IR and ^{29}Si MAS NMR spectra of GSN-1b, GSN-1c, and GSN-1d.

The FT-IR spectra of these samples (Fig. S14) showed bands corresponding to Ge–O–Ge stretching vibrations at $\sim 910\text{ cm}^{-1}$, which are characteristic for the cage germanoxane structure, along with bands assigned to the Si–O–Si stretching vibrations ($1050\text{--}1150\text{ cm}^{-1}$). The intensities of the bands due to the vinyl groups (1596 cm^{-1}) in **TEA-GeD4R** and Si–H groups ($2100\text{--}2200\text{ cm}^{-1}$)⁸ of the oligosiloxanes significantly decreased, which indicated the progress of the hydrosilylation reaction.

The ^{29}Si MAS NMR spectra of these samples (Fig. S15) showed signals at $\delta \sim 15\text{ ppm}$, which were assigned to $(\text{GeO})\text{SiMe}_2\text{CH}_2\text{--}$ formed during the hydrosilylation reaction. The signals due to the oligosiloxane linkers were also observed. **GSN-1b** (Fig. S15b) exhibited signals assigned to $\text{Si}(\text{OSi})_3\text{CH}_2\text{--}$ ($\delta = -65.6\text{ ppm}$)⁹ formed via the hydrosilylation reaction and unreacted $\text{SiH}(\text{OSi})_3$ ($\delta = -83.8\text{ ppm}$).⁹ The broad signal observed at around -103 ppm was probably attributed to the Si–OH groups formed via the oxidation of the Si–H groups and Si–O–Si bond formed via further condensation. The presence of Si–OH groups^{10,11} was also indicated by the broad band at $\sim 3000\text{ cm}^{-1}$ in the FT-IR spectrum (Fig. S14g). **GSN-1c** (Fig. S15c) exhibited signals assigned to $\text{Si}(\text{OSi})_2\text{MeCH}_2\text{--}$ ($\delta = -17.8\text{ ppm}$)¹² formed via the hydrosilylation reaction and the residual $\text{SiH}(\text{OSi}_2)\text{Me}$ groups ($\delta = -33.7\text{ ppm}$).¹² **GSN-1d** (Fig. S15d) exhibited a signal corresponding to $(\text{SiO})\text{SiMe}_2\text{CH}_2\text{--}$ ($\delta = 8.1\text{ ppm}$).¹² The small D₂ signal assigned to $\text{Si}(\text{OSi})_2\text{Me}_2$ ($\delta = -22.1\text{ ppm}$) was possibly formed by the conversion of the SiH groups into SiOH groups, followed by a condensation reaction during or after the hydrosilylation step.

Although the Si–Vi groups in **TEA-GeD4R** were fully reacted when M₂ was used as the linker, small signals corresponding to $(\text{GeO})\text{SiMe}_2\text{Vi}$ were observed at $\delta \sim 0\text{ ppm}$ ¹ when T₈ and D₄ were used. The ratios of reacted silyl groups/unreacted silyl groups in **GSN-1b** and **GSN-1c** were 1.6 and 7.0, indicating that 62 and 88% of the Si–Vi groups undergo the reaction, respectively. In addition, the oligosiloxane/cage germanoxane ratio was calculated. The integral ratios of the signals derived from the oligosiloxane linkers (T₈, D₄, and M₂) to those derived from **TEA-GeD4R** were 1.6, 1.1, and 1.0, respectively, indicating that the oligosiloxane/germanoxane ratios were 1.6, 2.2, and 4.0, respectively.

The oligosiloxane/germanoxane ratios of **GSN-1c** and **GSN-1d** were almost the same as those of the starting mixtures. However, the oligosiloxane/germanoxane ratio of **GSN-1b** was quite different from that of the starting mixture. As explained in the second paragraph above, the formation of silanol groups due to the side reaction of SiH group of T₈ and the following condensation to siloxane bonds caused the cross-linking between T₈ cages, resulted in the high ratio of T₈. The low yields of **GSN-1c** and **GSN-1d** were probably due to the removal of the low-molecular weight products by the washing procedures (see Experimental details).

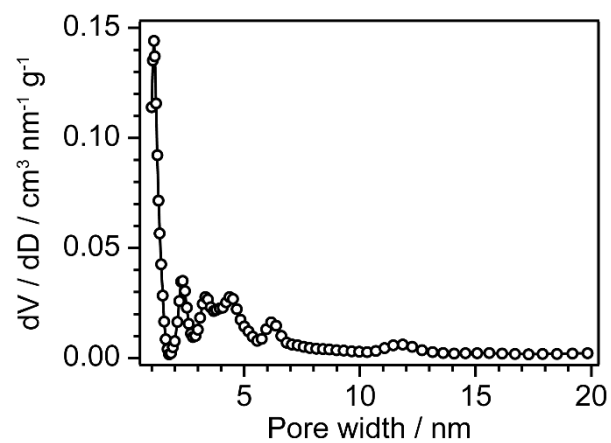


Fig. S16 Pore size distribution of **GSN-1b**.

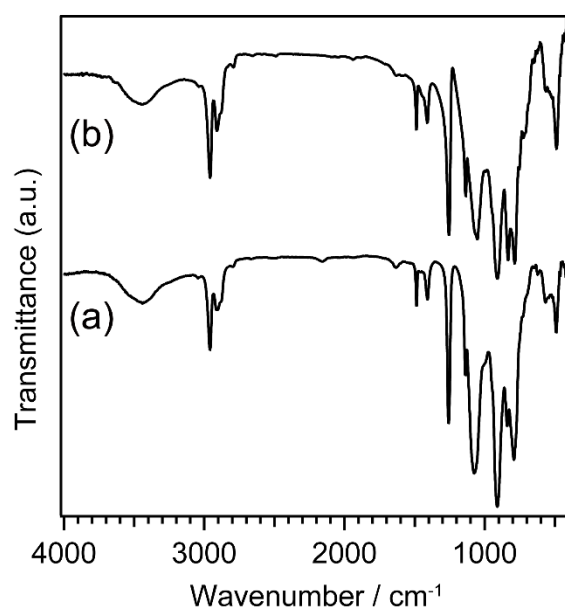


Fig. S17 FT-IR spectra of (a) **TMA-GSN-1c** and (b) **TMA-GSN-1d**.

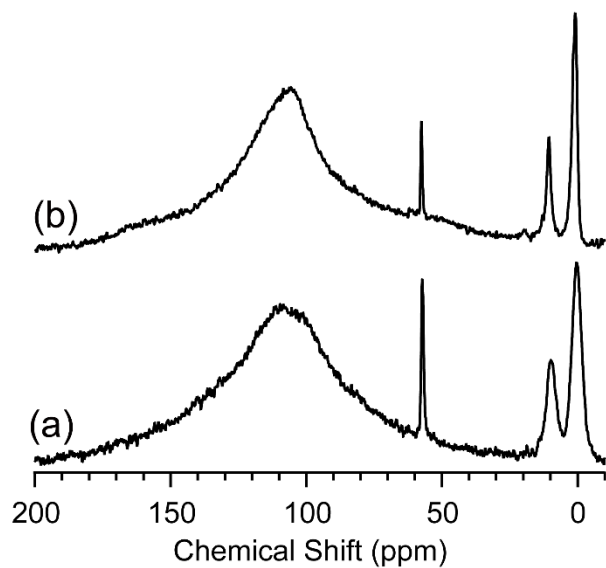


Fig. S18 ^{13}C MAS NMR spectra of (a) TMA-GSN-1c and (b) TMA-GSN-1d. A broad carbon background signal attributable to the probe was observed at 100–120 ppm due to the low carbon content.

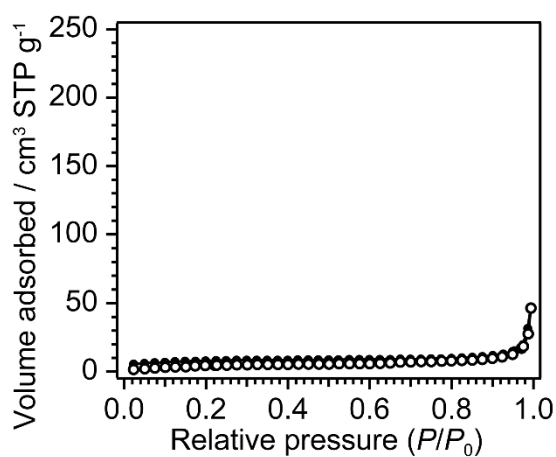


Fig. S19 N_2 adsorption–desorption isotherms of TMA-GSN-1c. The open and filled symbols denote adsorption and desorption, respectively.

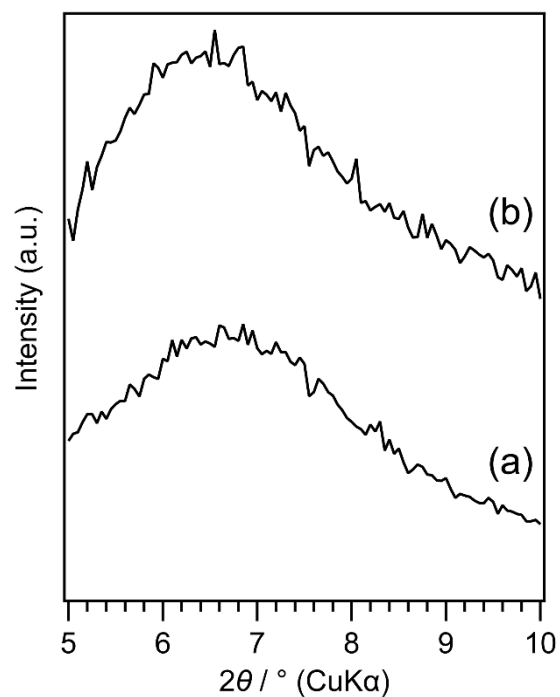


Fig. S20 XRD patterns of (a) **GSN-1c** and (b) **GSN-1c** with a drop of ethanol.

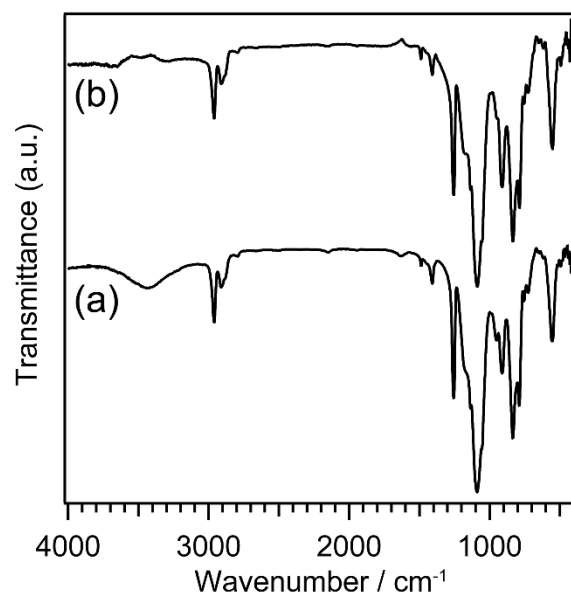


Fig. S21 FT-IR spectra of (a) **GSN-1a** and (b) **GSN-2a** treated with a mixed solution of TMACl, ethanol, and H₂O.

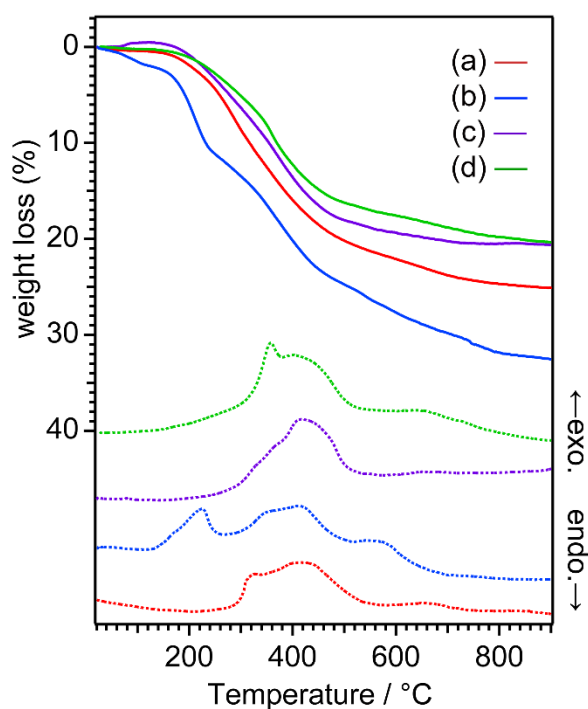


Fig. S22 TG-DTA curves of (a) **GSN-1a**, (b) **GSN-2a**, (c) **TMA-GSN-1a**, and (d) **TMA-GSN-2a**. The solid and dashed lines denote TG and DTA curves, respectively.

References

- 1 N. Sato, T. Hayashi, K. Tochigi, H. Wada, A. Shimojima and K. Kuroda, *Chem. Eur. J.*, 2019, **25**, 7860.
- 2 N. Sato, Y. Kuroda, T. Abe, H. Wada, A. Shimojima and K. Kuroda, *Chem. Commun.*, 2015, **51**, 11034.
- 3 P. A. Agaskar, *Inorg. Chem.*, 1991, **30**, 2707.
- 4 C. P. Rosenau, B. J. Jelier, A. D. Gossert and A. Togni, *Angew. Chem. Int. Ed.*, 2018, **57**, 9528.
- 5 K. Momma and F. Izumi, *J. Appl. Crystallogr.*, 2011, **44**, 1272.
- 6 W. Chaikittisilp, A. Sugawara, A. Shimojima and T. Okubo, *Chem. Eur. J.*, 2010, **16**, 6006.
- 7 Y. Du, M. Unno and H. Liu, *ACS Appl. Nano Mater.*, 2020, **3**, 1535.
- 8 G. J. Janz and Y. Mikawa, *Bull. Chem. Soc. Jpn.*, 1961, **34**, 1495.
- 9 C. Zhang, F. Babonneau, C. Bonhomme, R. M. Laine, C. L. Soles, H. A. Hristov and A. F. Yee, *J. Am. Chem. Soc.*, 1998, **120**, 8380.
- 10 G. I. Harris, *J. Chem. Soc.*, 1963, 5978.
- 11 J. Beckmann, A. Duthie, G. Reeske and M. Schürmann, *Organometallics*, 2004, **23**, 4630.
- 12 D. Hoebbel, I. Pitsch and D. Heidemann, *Z. Anorg. Allg. Chem.*, 1991, **592**, 207.